Patterned Production of Silver–Mesoporous Titania Nanocomposite Thin Films Using Lithography-Assisted Metal Reduction

Eduardo D. Martínez, Martín G. Bellino,* and Galo J. A. A. Soler-Illia*

Gerencia de Química, CNEA, Centro Atómico Constituyentes, Avenida Gral Paz 1499, San Martín B1650KNA, Argentina

ABSTRACT A simple method that allows selective positioning of nanoparticles into mesoporous monolayer or multilayer thin films is presented. This technique applies UV lithography in order to bring about in situ light-induced reduction of silver in templated cavities of TiO$_2$. The nanoparticle lithography presented here provides a novel approach to hierarchical lithography patterning for multifunctional devices.

KEYWORDS: patterning • metal nanoparticles • mesoporous films • UV lithography • photodeposition

The fabrication of multiscale nanostructures using a combination of methods is a growing field of interdisciplinary research. Advances in the fabrication of nanoscale devices will depend on the ability to synthesize, deposit, and position nanoobjects in suitably designed substrates. Building nanomaterials controlled in several length scales is a major technological challenge toward exploiting the improved functionality that arises from combining the positional order and the intrinsic properties of building blocks. Nanoparticles (NPs) have attracted great interest because they possess unique optical, electrical, magnetic, and catalytic properties. The highly controlled confined spaces of mesoporous materials (1) are excellent host matrixes for NPs (2), aiming at improving the NP stability, which is a necessary feature for practical applications (3). Metal NP–mesoporous thin film (MTF) nanocomposite systems present special interest because of the synergic properties of both NP and MTFs. In particular, mesopores constitute highly controlled nanoreactors for NP. The size-dependent NP properties, tuned by pore size, combined with an accessible and well-defined mesopore system, and the transparency and optimal transport properties of MTF present an enormous potential in fields such as catalysis (4), selective membranes (5), or ultrasensitive sensor platforms based in surface plasmon resonance (6).

Several soft approaches to obtain these novel nanocomposites have been reported: direct incorporation of NPs into the mesoporous materials, embedding of preformed NPs, and salt impregnation followed by reduction (2, 3).

A natural and desired evolution in NP–MTF composites is the possibility of fabricating arbitrary patterns of NP arrays within MTFs. This capability will allow for applications that require a precise spatial location of nanospecies such as in microfluidics, microarrays, nanoelectronic circuits, chemical and biological multisensor devices, lab-on-chip, optical switches, etc.

Photoreduction of metals on photoactive oxide matrixes is a promising route toward microscale patterning. It is well-known that the UV-excited electrons in the conduction band of TiO$_2$ can assist the reduction of Ag$^+$ ions to form metallic silver particles (7); this property is used for depositing silver NPs on the surface of nanostructured titania films (8).

In this work, we produce highly controlled micron-scale patterns with arbitrary shape composed of silver NPs placed into the pore systems of MTFs, either monolayer TiO$_2$ or bilayer SiO$_2$/TiO$_2$. Controlled positioning of NPs was successful in a single operation, using a lithographic method to assist selective silver photodeposition.

Metal NP–MTF nanocomposites were prepared using the well-known method of impregnation followed by reduction: in the first step, polymer-templated 150-nm-thick MTFs with pore structure derived from $Im\bar{3}m$ cubic symmetry were deposited by dip-coating followed by thermal treatment (9). Subsequently, the films were immersed in a silver nitrate–ethanol–water solution for in situ photoreduction of Ag$^+$ ions by exposure to UV radiation (see the Experimental Section and the Supporting Information for details).

When titania-based MTFs immersed in an ethanol–water solution of AgNO$_3$ are irradiated with UV light for 1 min, the films developed an orange color, as shown in Figure 1A. Progressive reduction of the Ag$^+$ ions with increasing UV irradiation time was evident by a gradual and steady development of a brownish color evenly distributed throughout the film. The characteristic color and absorption spectra observed for MTF are due to surface plasmon resonance of silver NPs for TiO$_2$ MTF (Figure 1B), indicating that silver NPs readily form in the titania films. However, silica films exposed to Ag$^+$ and UV light for at least 1 h did not show any color change, and no plasmon absorption was observed (Figure 1B). These results suggest that the titania framework is essential for the (photo)reduction process of Ag$^+$ in the
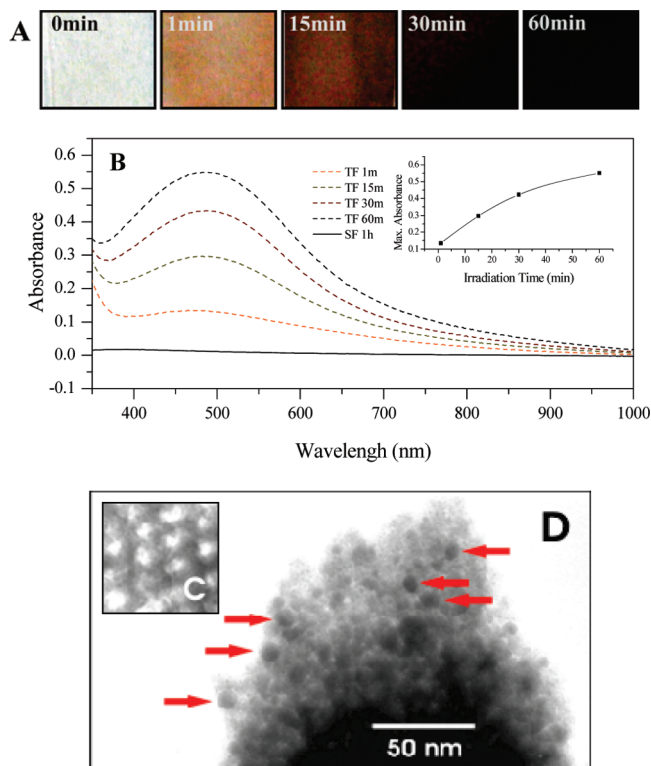
FIGURE 1. (A) Photography of F127-templated titania films exposed to a AgNO₃ solution under UV irradiation for variable periods (1, 15, 30, and 60 min), showing the progressive reduction of Ag^+. (B) UV−vis absorption spectra of a F127-templated silica film exposed to UV irradiation for 1 h (black curve) and titania (color curves) exposed for variable periods. The inset shows the variation of the absorbance at the plasmon peak maximum. (C and D) TEM images before and after 30 min of exposure. The arrows indicate the presence of well-defined NPs.

presence of ethanol; this effect is well-known in the literature (7). It is worth mentioning that the photocatalytic activity is highly dependent on the TiO_2 crystallinity. In our case, samples were typically deposited onto glass slides. It has been reported that glass-deposited mesoporous titania films calcined at 350 °C are mostly amorphous, and only present a minor fraction of Ti^{IV} sites with an anatase-like environment; however, these films present photoactive character (10).

Transmission electron microscopy (TEM) analysis of monolayer titania MTF showed homogeneous silver NP deposition with a major diameter of ca. 10 nm in the mesopores (Figure 1C,D), for irradiation times as short as 1 min. The NP loading is greater for longer exposure times, consistent with the observed color changes and UV−vis absorption spectroscopy trends. Energy-dispersive spectrometry (EDS) spectra of thoroughly rinsed films after exposure to UV corroborate a significant and continuous increase in the amount of silver contained in the MTF along the exposure time. No diffraction corresponding to crystalline particles was observed for the silver NP−MTF produced under our experimental conditions, by either X-ray diffraction analysis or electron diffraction, suggesting that mostly amorphous silver particles were obtained. Amorphous or very poorly crystalline particles could be a consequence of a very fast light-triggered NP nucleation process in the
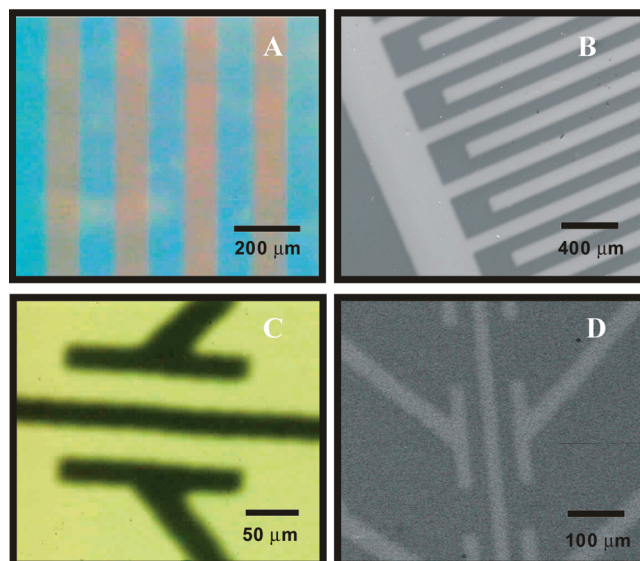

FIGURE 2. Reduction of Ag^+ using different masks to pattern the mesoporous infiltration. (A) Optical image of the monolayer TiO_2 mesoporous film after 1 min of exposure. (B) SEM image of the sample shown in A. (C) Optical image of a bilayered film SiO_2/TiO_2 after 30 min of UV exposure. (D) SEM image in backscattered electron mode for the sample shown in part C.

presence of a mild reducing agent such as ethanol. These conditions have also been reported in the production of silver nanocolloids by sonochemical or microwave synthesis routes (11). Experiments are in due course to investigate possible pathways to nanocrystalline silver upon aging.

Taking advantage of the latent properties described above for "drawing" with NPs in the MTF, we used this photolithography process for transferring geometrical shapes on a printed mask into the pores of MTF. UV radiation leads to the formation and localization of silver NPs only in the exposed areas.

Optical and scanning electron microscopy (SEM) images in Figure 2 display typical arrangements that were created from the simple photodeposition process using a polymeric mask (see the Experimental Section for details); photolithography provides the flexibility to create NP patterns of different shapes and sizes in a very simple and cost-effective manner. Parts A and B of Figure 2 show that silver NP patterns are readily deposited within the titania pore films after just 1 min of exposure time. The negative of the mask pattern is crisply transferred to the titania film. The samples were observed in an optical microscope in both bright-field (BF) and dark-field (DF) modes. While BF shows the reflection image, DF will show light scattered from surface irregularities. In films with 1 min of exposure, the field of view in the DF mode was completely black; however, the BF image shows a well-defined pattern, suggesting that the NPs are primarily formed within the mesopores and not deposited on the surface. With longer UV exposure, the contrast became sharper in the BF mode and an image became clear in the DF mode as well because of the formation of a continuous silver film on the surface. SEM analysis (Figure 2B) also demonstrates that the lithographic method allowed for patterned deposition of silver NP arrays in the titania
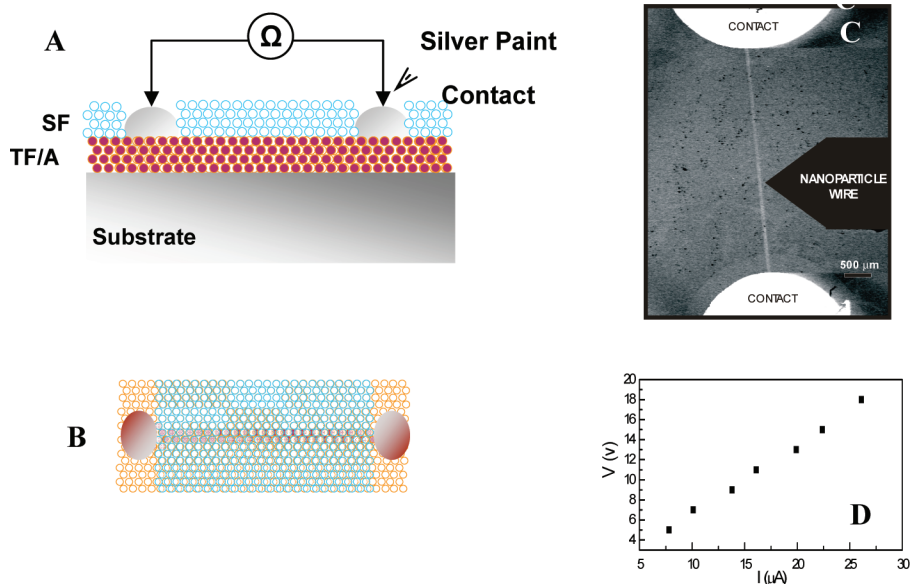
FIGURE 3. (A) Side scheme of the composite structure of the bilayer film submitted to electrical resistant measurement. (B) Top-view scheme of the microwire composed of silver NPs. (C) SEM image of the sample presenting a patterned NP wire. (D) Current−voltage response curve of a silver NP wire produced after 60 min of UV irradiation of the bilayer shown in Figure S1 in the Supporting Information.

mesopores. The UV-irradiated areas appeared bright due to the higher electron density of deposited silver NPs. Conversely, dark areas in unexposed sites were attributed to the absence of NPs.

Therefore, silver NP can be readily produced within titania MTFs and not in silica matrixes. This differential reactivity toward photoreduction can be exploited in order to generate silver NP within a well-defined film in a bilayer or multilayer, as was previously reported with selective chemical reduction (12). UV−vis spectra for silver produced in F127-templated TiO_2/SiO_2 bilayers (i.e., substrate−titania−silica) are similar to those obtained for titania monolayers (Figure S1 in the Supporting Information), suggesting selective NP photodeposition into the TiO_2 layer. Parts C and D of Figure 2 demonstrate that arbitrary patterned arrays of NPs can also be formed in a bilayered TiO_2/SiO_2 mesoporous film. DF optical images showed that silver particle formation on surfaces was inhibited, even at longer irradiation times. In the bilayer system, where the TiO_2 layer is covered by a SiO_2 layer, the presence of silver in the bottom layer was only revealed by imaging the backscattered electrons in SEM analysis.

These features demonstrate that the well-defined observed pattern obtained by lithography is attributable to the presence of silver NP only in the TiO_2 layer. The mesoporous SiO_2 top film allows Ag^+ to access the titania pore system, representing thus a penetrable coating, which prevents formation of a continuous metal film at the surface. It is worth mentioning that similar behaviors are also obtained by changing TiO_2 for ZrO_2 in the bilayer films, although silver NP formation rates are slower.

In order to be able to integrate NP for potential applications in electronic devices, it is desirable to generate conductive NP-based wires. We performed preliminary electrical conductivity experiments to prove the potential of these nanolayer films (see the Supporting Information for details).

For bilayer titania−silica films exposed to UV light for 1 h, an important increase in the conductivity is observed (see Figure 3). The conductivity was many orders of magnitude lower than that of bulk silver: a resistivity of approximately $0.1 \, \Omega \cdot cm$ was measured, in good agreement with the literature for characteristic values in the arrangement of silver NPs (13). The mesoporous film without silver NP is not conductive; therefore, any conductivity observed was attributed to silver NP loading. We believe that this behavior results from the limited electrical contact between the silver NPs. Further experiments are being conducted to improve the connectivity within particles. Interestingly, silver NP arrays become conductive only after a certain silver loading is attained. Pore volume filling was estimated from EDS measurements, according to previous results (12). In our case, an appreciable conductivity was observed only after 60 min of irradiation, where the filling fraction reached 50 %. Coincidently, a red shift in the silver plasmon resonance is observed (see the maximum indicated by an arrow in Figure S1A in the Supporting Information). These features suggest that a percolation of silver NP between the mesopores providing interparticle connectivity is necessary in order to obtain electronic conduction.

In summary, we have reported for the first time a very simple lithographic method that allows the creation of nanostructured metal patterns within MTFs with arbitrary shape on the submicron scale. This work combines conventional UV lithography (a top-down method) with in situ metal NP formation in templated cavities (a bottom-up method). We have shown that the choice of the inorganic framework is essential for the formation of these patterns. This leads to the possibility of creating complex patterned systems in MTF multilayers. Conditions can be optimized in order to attain a variable metal filling in a given region of a thin film. This advanced methodology provides a novel approach to hierarchical lithographic patterning compatible with the tech-

Scheme 1. Schematic Illustration of the Lithographic Procedure That Induces the Selective Reduction of Ag$^+$ Ions inside the MTF Immersed in a Ag$^+$ Solution (Left, Titania Monolayer; Right, SiO$_2$/TiO$_2$ Bilayer Films)
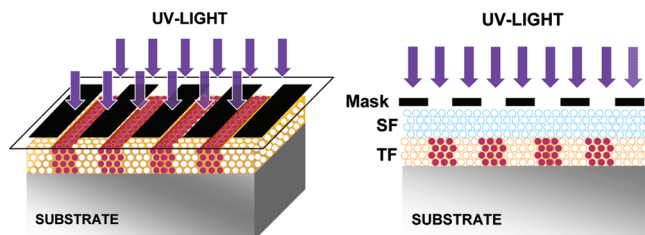
niques and substrates used in the sensor and microelectronics industry. Lithographic methods with better intrinsic resolution or two-photon techniques may be used for an additional improvement in the accuracy of the method (14). The NP photolithography route presented here is indeed a straightforward multiscale patterning method to include reactive NPs within a stable and accessible matrix. This opens a path to generate nanostructured arrangements with arbitrary shape for applications in catalysis, microarrays, lab-on-chip, photonic crystal waveguides, sensors, SERS detection, memories, nanocircuits, and other sophisticated devices needing a precise spatial location of functional NPs.

EXPERIMENTAL SECTION

Preparation of MTFs. Single-layer MTFs were deposited by dip-coating from ethanol–water acidic solutions containing an inorganic precursor and a polymeric template. Films were produced and processed under controlled environmental conditions and thermal treatment, following well-established protocols (see the Supporting Information for experimental details). The result of one deposition–consolidation step is a mesoporous layer with a typical thickness of 150 nm and an ordered cubic $Im\bar{3}m$ mesostructure (9). Titania films deposited on glass are mainly amorphous and contain minor domains with a local anatase structure after treatment at 350 °C (10).

Photodeposition of Silver NPs. In order to fill the pores of the mesoporous films, the film was immersed in a 1 M AgNO$_3$ water–ethanol solution (1:1 volume ratio) for 10 min under agitation in the dark to optimize metal infiltration. Subsequently, films were placed in a shallow plastic container. A few milliliters of the Ag$^+$ solution described above was added until the film was completely immersed. A polymeric mask (made by high-resolution laser jet printing on an acetate foil) was placed over the film before the solution was added. The mask stuck to the film because of capillary forces, and no adhesives were required. Finally, the container was placed 1 cm below the UV tube lamp (Phillips, 15 W, emission peak at 355 nm) for the desired time. After deposition, the mask was removed; the sample was retired from the bath and thoroughly rinsed with water and ethanol.

Supporting Information Available: Experimental details of the film synthesis, film characterization, and conductivity experiments, UV–vis absorption spectra of a silver-loaded TF–SF bilayer after progressive UV irradiation times, and Ag/Ti ratios obtained from EDS spectra performed in the silver-patterned zone. This material is available free of charge via the Internet at http://pubs.acs.org.

REFERENCES AND NOTES

(1) (a) Soler-Illia, G. J. A. A.; Sanchez, C.; Lebeau, B.; Patarin, J. *Chem. Rev.* **2002**, *102*, 4093. (b) Sanchez, C.; Boissière, C.; Grosso, D.; Laberty, C.; Nicole, L. *Chem. Mater.* **2008**, *20*, 682.

(2) (a) Bronstein, L. M. *Top. Curr. Chem.* **2003**, *226*, 55. (b) Plyuto, Y.; Berquier, J. M.; Jacquiod, C.; Ricolleau, C. *Chem. Commun.* **1999**, 1653. (c) Zhu, J.; Kónya, Z.; Puntes, V. F.; Kiricsi, I.; Miao, C. X.; Ager, J. W.; Alivisatos, A. P.; Somorjai, G. A. *Langmuir* **2003**, *19*, 4396. (d) Pérez, M. D.; Otal, E.; Bilmes, S. A.; Soler-Illia, G. J. A. A.; Crepaldi, E. L.; Grosso, D.; Sanchez, C. *Langmuir* **2004**, *20*, 6879. (e) Andersson, M.; Birkedal, H.; Franklin, N. R.; Ostomel, T.; Boettcher, S.; Palmqvist, A. E. C.; Stucky, G. D. *Chem. Mater.* **2005**, *17*, 1409. (f) Pénard, A. L.; Gacoin, T.; Boilot, J. P. *Acc. Chem. Res.* **2007**, *40*, 895. (g) Fan, H.; Yang, K.; Boye, D. M.; Sigmon, T.; Malloy, K. J.; Xu, H.; Lopez, G. P.; Brinker, C. J. *Science* **2004**, *304*, 567. (h) Kumai, Y.; Tsukada, H.; Akimoto, Y.; Sugimoto, N.; Seno, Y.; Fukuoka, A.; Ichikawa, M.; Inagaki, S. *Adv. Mater.* **2006**, *18*, 760.

(3) (a) Cai, W.; Hofmeister, H.; Rainer, T. *Physica E* **2001**, *11*, 339. (b) Tripp, R. A.; Dluhy, R. A.; Zhao, Y. *Nanotoday* **2008**, *3*, 3. (c) Lombardi, I.; Cavallotti, P. L.; Carraro, C.; Maboudian, R. *Sens. Actuators, B* **2007**, *125*, 353. (d) Yang, C.; Kalwei, M.; Schüth, F.; Chao, K. *Appl. Catal., A* **2003**, *254*, 289. (e) Wang, H. W.; Lin, H. C.; Kuo, C. H.; Cheng, Y. L.; Yeh, Y. C. *J. Phys. Chem. Solids* **2008**, *69*, 633.

(4) (a) Rolison, D. R. *Science* **2003**, *299*, 1698. (b) Cortial, G.; Siutkowski, M.; Goettmann, F.; Moores, A.; Boissière, C.; Grosso, D.; Le Floch, P.; Sanchez, C. *Small* **2006**, *2*, 1042.

(5) Levy, C.; Guizard, C.; Julbe, A. *Sep. Purif. Technol.* **2003**, *32*, 327.

(6) (a) Ko, H.; Singamaneni, S.; Tsukruk, V. V. *Small* **2008**, *4*, 1576. (b) Goettmann, F.; Moores, A.; Boissière, C.; Le Floch, P.; Sanchez, C. *Small* **2005**, *1*, 636. (c) Yang, Z.; Ni, W.; Kou, X.; Zhang, S.; Sun, Z.; Sun, L. D.; Wang, J.; Yan, C. H. *J. Phys. Chem. C* **2008**, *112*, 18895.

(7) (a) Chen, X.; Mao, S. *Chem. Rev.* **2007**, *107*, 2891. (b) Matsubara, K.; Kelly, K. L.; Sakaia, N.; Tatsuma, T. *Phys. Chem. Chem. Phys.* **2008**, *10*, 2263.

(8) Stathatos, E.; Lianos, P.; Falaras, P.; Siokou, A. *Langmuir* **2000**, *16*, 2398.

(9) (a) Crepaldi, E. L.; Soler-Illia, G. J. A. A.; Grosso, D.; Ribot, F.; Cagnol, F.; Sanchez, C. *J. Am. Chem. Soc.* **2003**, *125*, 9770. (b) Crepaldi, E. L.; Soler-Illia, G. J. A. A.; Grosso, D.; Sanchez, C. *New J. Chem.* **2003**, *27*, 9. (c) Angelomé, P. C.; Fuertes, M. C.; Soler-Illia, G. J. A. A. *Adv. Mater.* **2006**, *18*, 2397. (d) Cagnol, F.; Grosso, D.; Soler-Illia, G. J. A. A.; Crepaldi, E. L.; Babonneau, F.; Amenitsch, H.; Sanchez, C. *J. Mater. Chem.* **2003**, *13*, 61. (e) Fuertes, M. C.; López-Alcaraz, F. J.; Marchi, M. C.; Troiani, H. E.; Luca, V.; Míguez, H.; Soler-Illia, G. J. A. A. *Adv. Funct. Mater.* **2007**, *17*, 1247.

(10) Angelomé, P. C.; Andrini, L.; Calvo, M. E.; Requejo, F. G.; Bilmes, S. A.; Soler-Illia, G. J. A. A. *J. Phys. Chem. C* **2007**, *111*, 10886.

(11) (a) Salkar, R. A.; Jeevanandam, P.; Aruna, S. T.; Koltypin, Y.; Gedanken, A. *J. Mater. Chem* **1999**, *9*, 1333. (b) He, R.; Qian, X.; Yin, J.; Zhu, Z. *J. Mater. Chem.* **2002**, *12*, 3783. (c) Pol, V. G.; Srivastava, D. N.; Palchik, O.; Palchik, V.; Slifkin, M. A.; Weiss, A. M.; Gedanken, A. *Langmuir* **2002**, *18*, 3352.

(12) Fuertes, M. C.; Marchena, M.; Marchi, M. C.; Wolosiuk, A.; Soler-Illia, G. J. A. A. *Small* **2009**, *5*, 272.

(13) Wu, M.; Kuga, S.; Huang, Y. *Langmuir* **2008**, *24*, 10494.

(14) (a) Gates, B. D.; Xu, Q.; Stewart, M.; Ryan, D.; Willson, C. G.; Whitesides, G. M. *Chem. Rev.* **2005**, *105*, 1171. (b) Falcaro, P.; Costacurta, S.; Malfatti, L.; Takahashi, M.; Kidchob, T.; Casula, M. F.; Piccinini, M.; Marcelli, A.; Marmiroli, B.; Amenitsch, H.; Schiavuta, P.; Innocenzi, P. *Adv. Mater.* **2008**, *20*, 1864. (c) Innocenzi, P.; Kidchob, T.; Falcaro, P.; Takahashi, M. *Chem. Mater.* **2008**, *20*, 607.

AM900018J